J Intell Robot Syst (2010) 57:217–231
DOI 10.1007/s10846-009-9382-2

A Vision-Based Automatic Landing Method for Fixed-Wing UAVs

Sungsik Huh · David Hyunchul Shim

Received: 1 February 2009 / Accepted: 1 August 2009 / Published online: 23 October 2009

Abstract In this paper, a vision-based landing system for small-size fixed-wing unmanned aerial vehicles (UAVs) is presented. Since a single GPS without a differential correction typically provide position accuracy of at most a few meters, an airplane equipped with a single GPS only is not guaranteed to land at a designated location with a sufficient accuracy. Therefore, a visual servoing algorithm is proposed to improve the accuracy of landing. In this scheme, the airplane is controlled to fly into the visual marker by directly feeding back the pitch and yaw deviation angles sensed by the forward-looking camera during the terminal landing phase. The visual marker is a monotone hemispherical airbag, which serves as the arresting device while providing a strong and yet passive visual cue for the vision system. The airbag is detected by using color- and moment-based target detection methods. The proposed idea was tested in a series of experiments using a blended wing-body airplane and proven to be viable for landing of small fixed-wing UAVs.

Keywords Landing dome · Fixed-wing UAVs · Visual servoing · Automatic landing

1 Introduction

It is well known that the landing is the most accident-prone stage for both manned and unmanned airplanes since it is a delicate process of dissipating the large amount of kinetic and potential energy of the airplane in the presence of various dynamic and operational constraints. Therefore, commercial airliners heavily rely on instrument landing system (ILS) wherever available. As for UAVs, a safe and sound retrieval of

S. Huh (✉) · D. H. Shim
Department of Aerospace Engineering, KAIST, Daejeon, South Korea
e-mail: hs2@kaist.ac.kr
URL: http://unmanned.kaist.ac.kr

D. H. Shim
e-mail: hcshim@kaist.ac.kr

the airframe is still a significant concern. Typically, UAVs land manually by either internal or external human pilots on a conventional runway or arresting mechanisms. For manual landing, the pilot obtains visual cue by naked eye or through the live images taken by the onboard camera. Piloting outside of the vehicle needs a lot of practice due to the limited situation awareness. As a consequence, a significant portion of mishaps happen during the landing phase. Nearly 50% of fixed-wing UAVs such as Hunter and Pioneer operated by the US military suffer accidents during landing. As for Pioneer UAVs, almost 70% of mishaps occur during landing due to human factors [1, 2]. Therefore, it has been desired to automate the landing process of UAVs in order to reduce the number of accidents while alleviating the pilots' load.

There are a number of automatic landing systems currently in service. Global Hawk relies on a high-precision differential GPS during take-off and landing [3]. Sierra Nevada Corporation's UCARS or TALS[1] are externally located aiding systems consisting of a tracking radar and communication radios. It has been successfully used for landing of many military fixed-wing and helicopter UAVs such as Hunter or Fire Scout on runways or even on a ship deck. The information including the relative position or altitude of the inbound aircraft is measured by the ground tracking radar and relayed back for automated landing. Some UAVs are retrieved in a confined space using a special net, which arrests the vehicle flown manually by the external pilot. Scan Eagle is retrieved by a special arresting cable attached to the tall boom, to which the vehicle is precisely guided by a differential GPS.[2] These external aids listed above rely on special equipment and radio communication, which are not always available or applicable due to complexity, cost, or limits from operating environment. Therefore, automatic landing systems that are inexpensive, passive, and reliable are highly desired.

Vision-based landing has been found attractive since it is passive and does not require any special equipment other than a camera and a vision processing unit onboard. A vision-enabled landing system will detects the runway or other visual markers and guide the vehicle to the touchdown point. There are a range of previous works, theoretical or experimental, for fixed-wing and helicopter UAVs [4–6]. Notably, Barber et al. [7] proposed a vision-based landing for small fixed-wing UAVs, where visual marker is used to generate the roll and pitch commands to the flight controller.

In this paper, a BWB-shaped fixed-wing UAV is controlled to land automatically by using vision algorithms and relatively simple landing aids. The proposed method is shown to be viable without resorting to expensive sensors and external devices. The overall approach, its component technologies, and the landing aids including the landing dome and recovery net are described in Section 2. The vision algorithms including detection and visual servoing algorithm which enables airplane to land automatically are described in Section 3. Finally, the experiment results of vision-based landing test are shown to validate the algorithm in Section 4. In Section 5, conclusion and closing remarks are given.

[1] http://www.sncorp.com

[2] http://www.insitu.com/scaneagle

2 System Description

The proposed landing system consists of three major components: an inflated dome as a visual marker, a vision processing unit, and a flight controller using a visual servoing algorithm. In order to develop a low-cost landing system without expensive sensors or special supporting systems, the vision system is integrated with an MEMS-based inertial measurement unit (IMU) and a single GPS. Without a differential correction, the positioning accuracy of GPS is known to be a few meters horizontally and twice as bad vertically. Therefore, even if the position of the dome is accurately known, it will be still difficult to hit the dome consistently with the navigation system that has position error larger than the size of the landing dome.

For landing, with roughly estimated location of the dome, the airplane starts flying along a glide slope leading to the estimated position of the dome. When the vision system locks on the dome, the flight control switches from glide slope tracking to direct visual servoing, where the offset of the dome from the center of the image taken from the onboard front-looking camera is used as the error signals for the pitch and yaw control loops. In the following, detailed descriptions on the proposed approach are presented (Fig. 1).

2.1 Airframe and Avionics

The platform used in this research is a BWB-based UAV (Fig. 2). BWBs are known to carry a substantially large payload per airframe weight due to the extra lift generated by the airfoil-shaped fuselage. Our BWB testbed is constructed with sturdy expanded polypropylene (EPP), which is reinforced with carbon fiber spars embedded at strategic locations. The vehicle is resilient to shock and crash, a highly welcomed trait for the landing experiments in this paper.

This BWB has only two control surfaces at the trailing edge of the wing, known as elevons, which serve as both aileron and elevator. At the wingtips, winglets are installed pointing down to improve the directional stability. The vehicle has a DC brushless motor mounted at the trailing edge of the airframe, powered by Lithium-polymer cells. The same battery powers the avionics to lower the overall weight. The

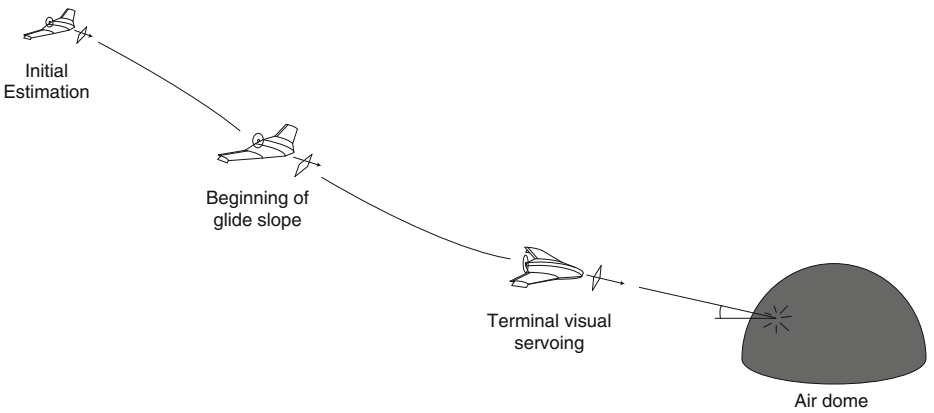

Fig. 1 Proposed dome-assisted landing procedure of a UAV

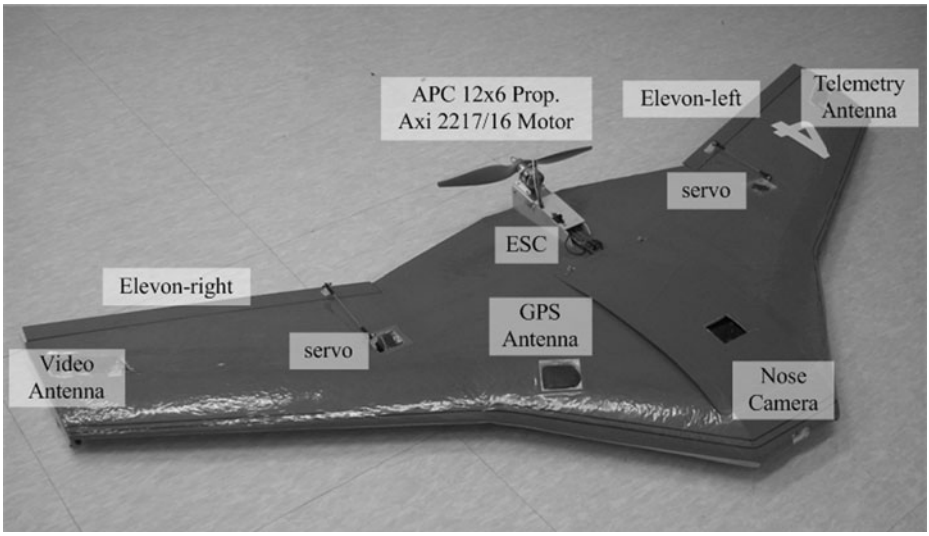

Fig. 2 The KAIST BWB (blended wing-body) UAV testbed

large payload compartment (30 × 15 × 7.5 cm) in the middle of the fuselage houses the flight computer, IMU, battery, and radio receiver. These parts are all off the shelf products.

The avionics of KAIST BWB UAV consists of a flight control computer (FCC), an inertial measurement unit(IMU), a GPS, and a servo controller module. Flight control computer is constructed using PC104-compatible boards due to their industry-grade reliability, compactness and expandability. The navigation system is built around a GPS-aided INS. U-blox Supersense 5 GPS is used for its excellent tracking capability even when the signal quality is low. Inertial Science's MEMS-IMU showed a robust performance during the flight. The vehicle communicates with the ground station through a high-bandwidth telemetry link at 900 MHz to reduce the communication latency (Table 1, Fig. 3).

The onboard vision system consists of a small forward-looking camera mounted at the nose of the airframe, a video overlay board, and a 2.4 GHz analog video transmitter with a dipole antenna mounted at a wingtip. Due to the payload limit, the image processing is currently done at the ground station, which also serves as the monitoring and command station. Therefore the image processing and vision algorithm results are transmitted back to the airplane over the telemetry link. Image processing and vision algorithms are processed on a laptop computer with Pentium Core2 CPU 2 GHz processor and 2 GB memory. Vision algorithm is written in MS Visual C++ using OpenCV library.[3] It takes 240 ms to process the vision algorithm at an image, then, the visual servoing command is transmitted back to the vehicle at 4 Hz, which is shown to be sufficient for the visual servoing problem considered in this research.

[3]Intel Open Source Computer Vision Library

Table 1 Specification of BWB testbed

Base platform	StingRay 60 by *Haak Works*[a]
	Blended wing-body (BWB)
Dimensions	Wing span: 1.52 m(W)
	Wing area: 0.52 m^2
	Aspect ratio: 4.43
Weight	2.6 kg (fully instrumented)
Powerplant	Axi 2217/16 DC brushless motor
	12 × 6 APC propeller
	Hacker speed controller X-40-SB-Pro
	Lithium-ion-polymer (3 S: 11.1 V 5,350 mAh)
Operation time	Over 10 min
Avionics	Navigation: single GPS-aided INS
	GPS: U-Blox Supersense 5
	IMU: inertial science MEMS IMU
	Differential/absolute pressure gauges
	Flight computer: PC104 Pentium-M 400 MHz
	Communication: 900 MHz Ethernet Bridge
Vision system	Color CCD camera (70 deg FOV)
	2.4 GHz analog transmitter
	Frame grabber: USB 2.0 analog video capture kit
Operation	Catapult-launch, body landing
Autonomy	Speed, altitude, heading, altitude hold/command
	Waypoint navigation
	Automatic landing

[a]http://www.haakworks.com

2.2 Landing Equipment

In order to land an airplane in a confined space, an arresting device is needed to absorb the kinetic energy in a relatively short time and distance. In this research, we propose a dome-shaped airbag, which offers many advantages for automatic landing scenarios.

The dome is constructed with sturdy nylon of a vivid red color, which provides a strong visual cue even at a long distance. It also absorbs the shock during the landing and therefore the vehicle would not need to make any special maneuver but simply fly into the dome at a low speed with a reasonable incident angle. The vision system runs a fast and reliable color tracking algorithm, suitable for high-rate visual servoing under various light conditions.

For operation, the bag is inflated within a few minutes by a portable electric blower or possibly by a gas-generating charge and transported to anywhere in a compact package after deflated. Using the hooks sewn around the bottom patch, it can be secured to the ground using pegs. Its dome shape allow landing from any direction without reinstallation while conventional arresting nets have to be installed to face the wind to avoid crosswind landing. Since this approach is vision-based, the landing dome is not equipped with any instruments, signal sources, or communication devices. Therefore it does not consume any power or emits energy that can be detected by adversaries.

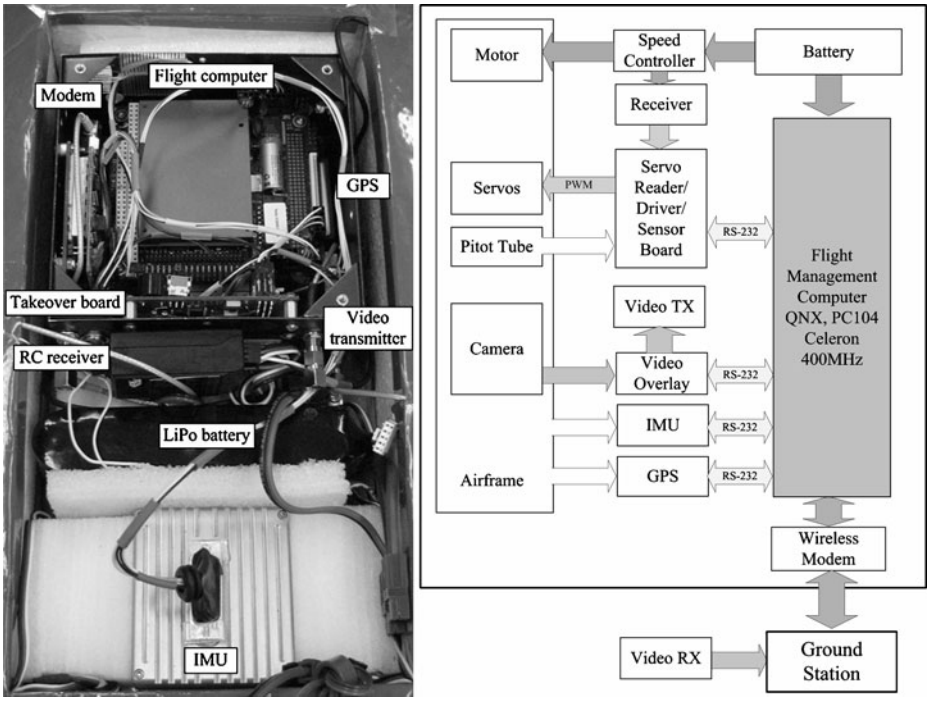

Fig. 3 Avionics and hardware architecture

In addition, a recovery net can be used to capture larger vehicles. In this case, the landing dome serves only as a visual cue and the recovery net is responsible for arresting the vehicle.

3 Vision Algorithms

The proposed vision algorithm consists of a color-based detection, a moment-based detection, and visual servoing. The color- and moment-based methods perform in a complementary manner to detect the landing dome more reliably. In the terminal stage of landing, the vehicle maneuvers by the visual servoing command only (Fig. 4).

3.1 Color-Based Target Detection

The dome's color is the strongest visual cue that distinguishes the target from other objects in the background. In RGB coding, a pixel at image coordinate (x, y) has three integers, (I_R, I_G, I_B), varying from 0 to 255, respectively. As the pixels that belong to the red dome vary quite large depending on lighting condition, shadow, color balance, or noise, a filtering rule is needed to determine whether a pixel

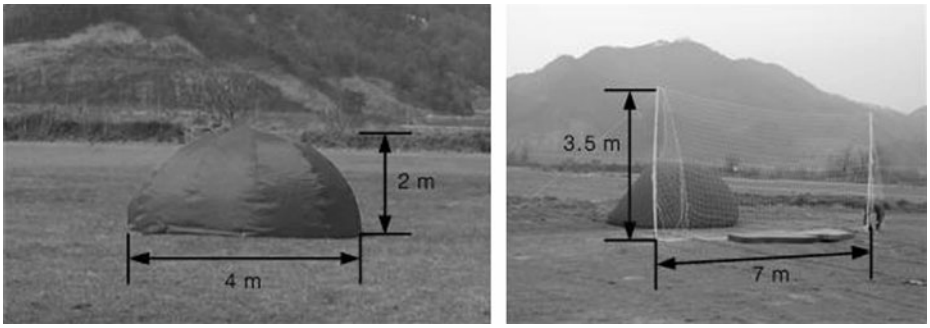

Fig. 4 Proposed landing dome and a recovery net

belongs to the dome or not. Based on many images of the dome taken under various conditions, the following filtering rule is proposed:

$$\begin{aligned} aI_B(x, y) &< I_R(x, y) \leq 255 \\ b\,I_G(x, y) &< I_B(x, y) \leq 255 \\ 0 \leq c &< I_R(x, y) \end{aligned} \tag{1}$$

where $(a, b, c) = (1.5, 1.5, 20)$. The threshold levels are chosen rather inclusively for detection of wider color range. Figure 5 visualizes the colors that are qualified as a dome using Eq. 1.

3.2 Moment-Based Target Detection

When multiple red objects are found by the color-based detection described above in a given image, another classification is needed to determine whether an object is

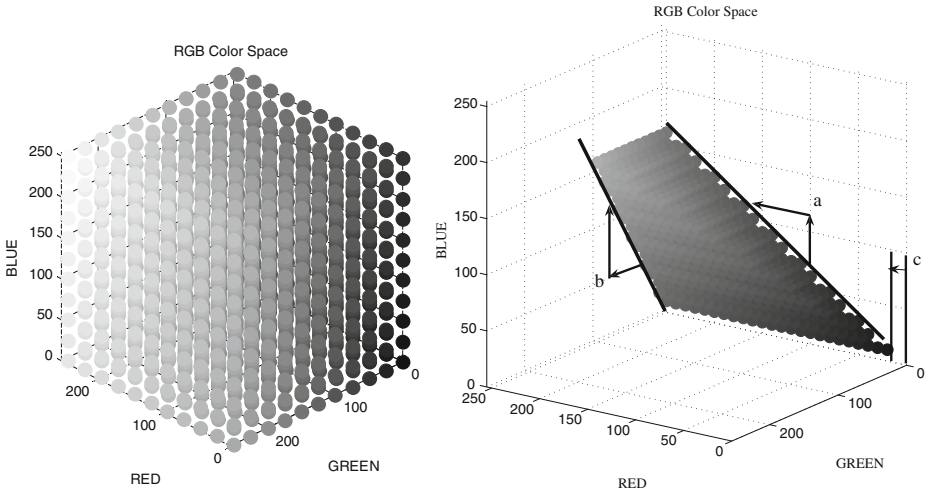

Fig. 5 Full RGB color space (*left*) and selected region by filtering rule (*right*)

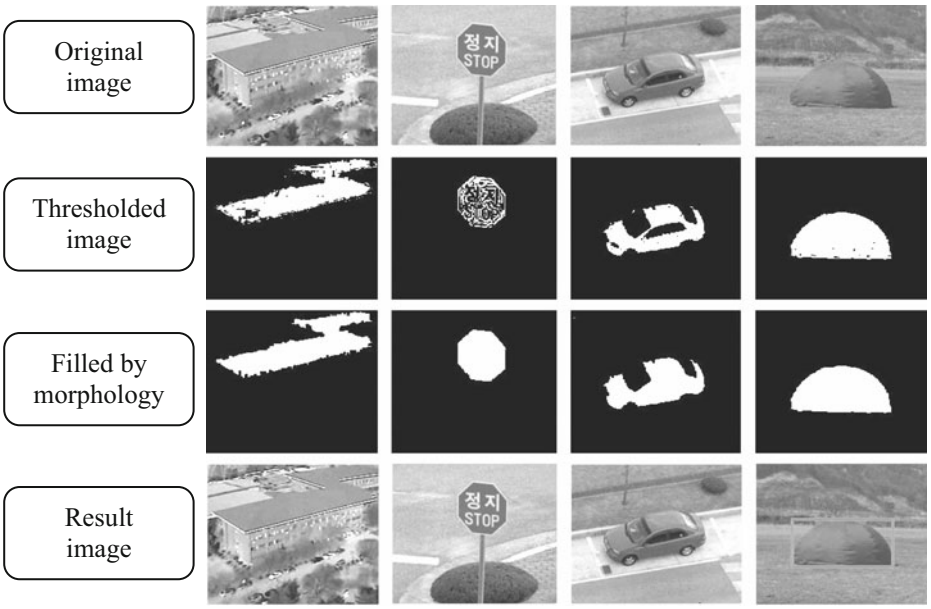

Fig. 6 Moment-based image processing procedure

indeed the landing dome or not. For this, an image moment-based filtering is devised. Among many algorithms such as template matching or image moment comparison, Hu's method [8, 9] is used since it is computationally efficient for high-rate detection needed for vision-based landing (Table 1).

Hu's moment consists of seven moment invariants derived from the first three central moments. In a gray image with pixel intensities $I(x, y)$, raw image moments M_{ij} are calculated by

$$M_{ij} = \sum_x \sum_y x^i y^j I(x, y). \tag{2}$$

Then simple image properties derived by raw moments include the area of image M_{00}, and its centroid $\{\bar{x}, \bar{y}\} = \{M_{10}/M_{00}, M_{01}/M_{00}\}$.

Central moments for digital image are defined as below

$$\mu_{ij} = \sum_x \sum_y (x - \bar{x})^p (y - \bar{y})^q f(x, y) \tag{3}$$

Table 2 Hu's moment value of various shapes in Fig. 6

	Roof	Road sign	Automobile	Landing dome
Hu's moment 1	0.48560	0.20463	0.27423	0.21429
Hu's moment 2	0.18327	0.00071	0.04572	0.01806
Hu's moment 3	0.01701	0.00009	0.00193	0.00106
Hu's moment 4	0.00911	0.00028	0.00098	0.00007

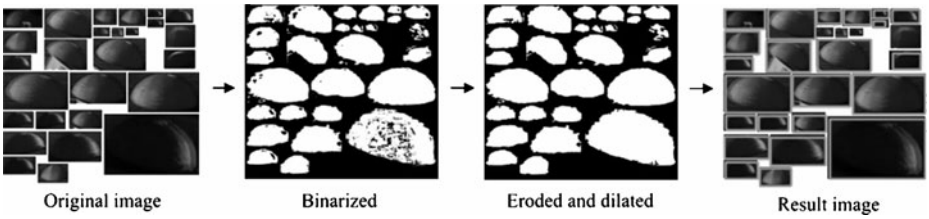

Fig. 7 Application of Hu's method to domes seen from various viewpoints

and the central moments of order up to the third order are given as

$$\begin{aligned}
\mu_{01} &= \mu_{10} = 0 \\
\mu_{11} &= M_{11} - \bar{x}M_{01} = M_{11} - \bar{y}M_{10} \\
\mu_{20} &= M_{20} - \bar{x}M_{10} \\
\mu_{02} &= M_{02} - \bar{y}M_{01} \\
\mu_{21} &= M_{21} - 2\bar{x}M_{11} - \bar{y}M_{20} + 2\bar{x}^2 M_{01} \\
\mu_{12} &= M_{12} - 2\bar{y}M_{11} - \bar{x}M_{02} + 2\bar{y}^2 M_{10} \\
\mu_{30} &= M_{30} - 3\bar{x}M_{20} + 2\bar{x}^2 M_{10} \\
\mu_{03} &= M_{03} - 3\bar{y}M_{02} + 2\bar{y}^2 M_{01}
\end{aligned} \tag{4}$$

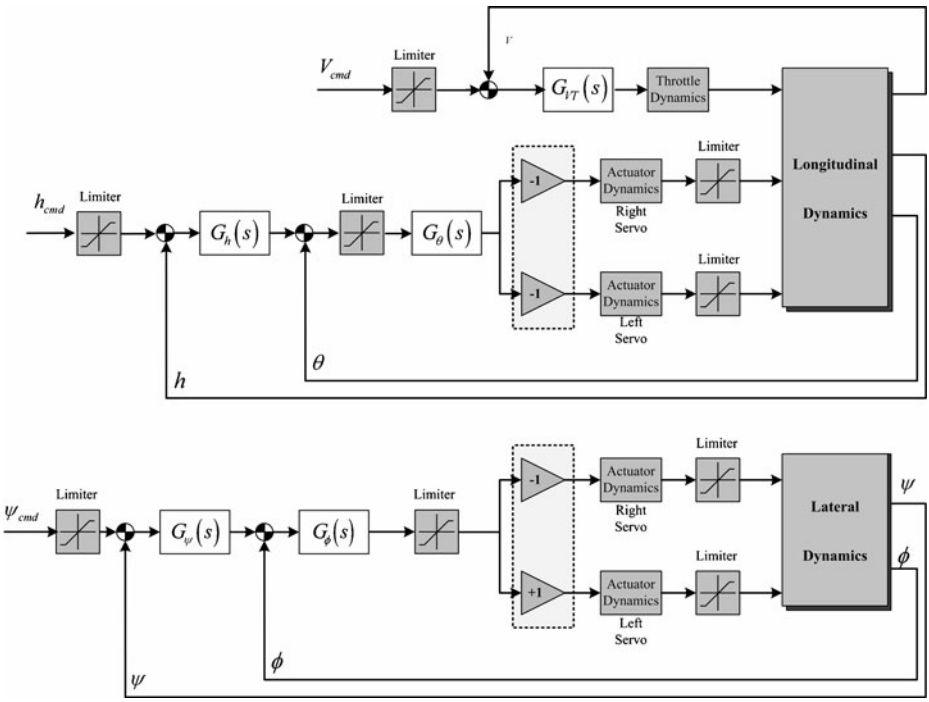

Fig. 8 Autopilot loops for longitudinal (*top*) and lateral dynamics (*bottom*) of airplane

In order to make the moments invariant to both translation and changes in scale, the following formula is used to divide the corresponding central moment by the properly scaled moment.

$$\eta_{ij} = \frac{\mu_{ij}}{\mu_{00}^{((i+j+2)/2)}} \tag{5}$$

Since the dome is projected to be somewhere between a semicircle to a full circle, its Hu's moments would not vary too much regardless of the distance and the viewing angle. Therefore Hu's moment can be a good invariant characterization of a target shape. Using the second- and third-order moments given in Eq. 5, the following Hu's image moments that are invariant to translation, rotation, and scale are derived:

$$\begin{aligned}
\phi_1 &= \eta_{20} + \eta_{02} \\
\phi_2 &= (\eta_{20} - \eta_{02})^2 + (2\eta_{11})^2 \\
\phi_3 &= (\eta_{30} - 3\eta_{12})^2 + (3\eta_{21} - \eta_{03})^2 \\
\phi_4 &= (\eta_{30} - \eta_{12})^2 + (\eta_{21} + \eta_{03})^2
\end{aligned} \tag{6}$$

In this paper, only four image moments are used for detection.

Hu's moments approach is applied to various red objects seen from air as shown in Fig. 6 and their moment values are listed in Table 2. The rooftop and the automobile in Fig. 6 has relatively larger Hu's moments while the road sign and the landing dome have comparable first moments due to their round shapes. The higher-order moments of the road sign has much smaller values than those of landing dome since the road sign has a smaller area for given number of pixels. Although the landing dome seen directly above would look much similar to the road sign, such cases are excluded because the camera is mounted to see only the side of the dome during landing.

In Fig. 7, the image processing results of landing domes seen from various viewpoints. Once a database of Hu's moments of these domes was built, the average, standard deviation, and minimum/maximum values of landing dome can be determined. Based on these values, the blob with the largest area in a given image is finally declared as the landing dome. In case of all candidates are not in the proper range of Hu's moments, the algorithm concludes that a landing dome does not exist in that image.

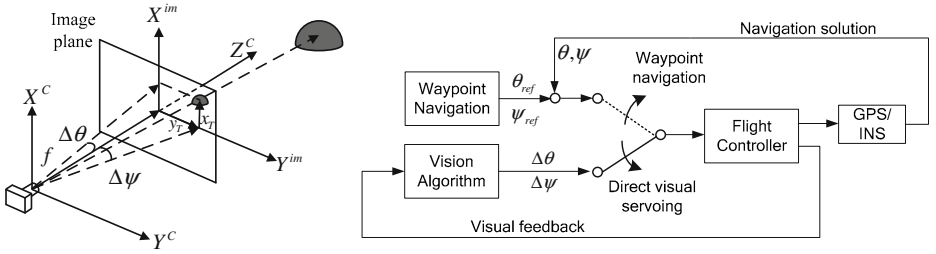

Fig. 9 Visual servoing scheme

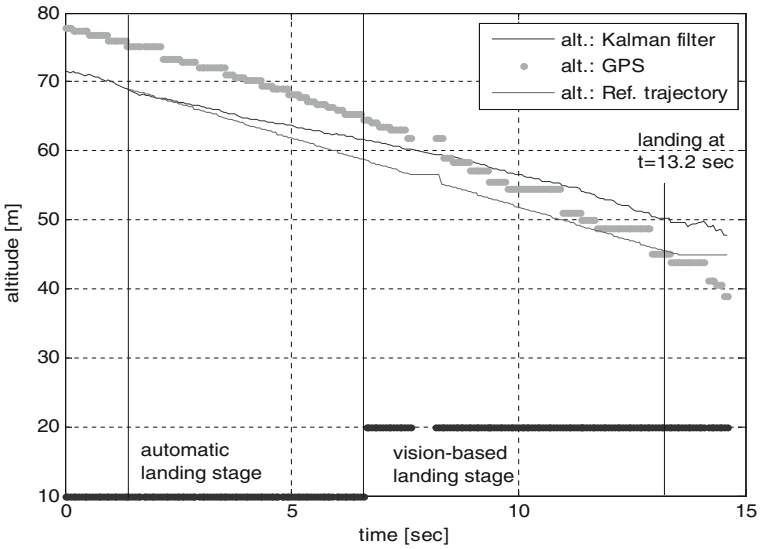

Fig. 10 Experiment result of vision-based landing: vehicle altitude

3.3 Visual Servoing

Visual servoing is a method to control a robot using computer vision. The robot is controlled by the error of features between the desired image and current image. The visual servoing method can be applied to the fixed-wing UAV such that the vehicle is controlled by the pitch and roll angle errors estimated from an image as shown in Fig. 8.

As illustrated in Fig. 9, the offset of the landing dome from the center of the image represents the heading and pitch deviation.

$$\begin{aligned} \Delta\psi &= \arctan\left(y_T / f\right) \\ \Delta\theta &= \arctan\left(x_T / f\right) \end{aligned} \tag{7}$$

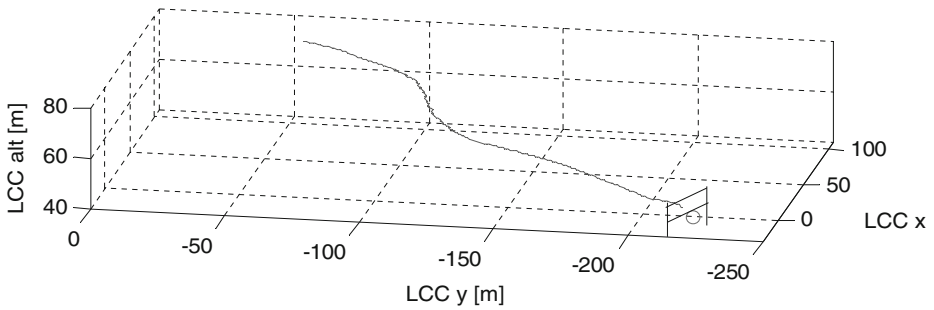

Fig. 11 Experiment result of vision-based landing: 3D trajectory

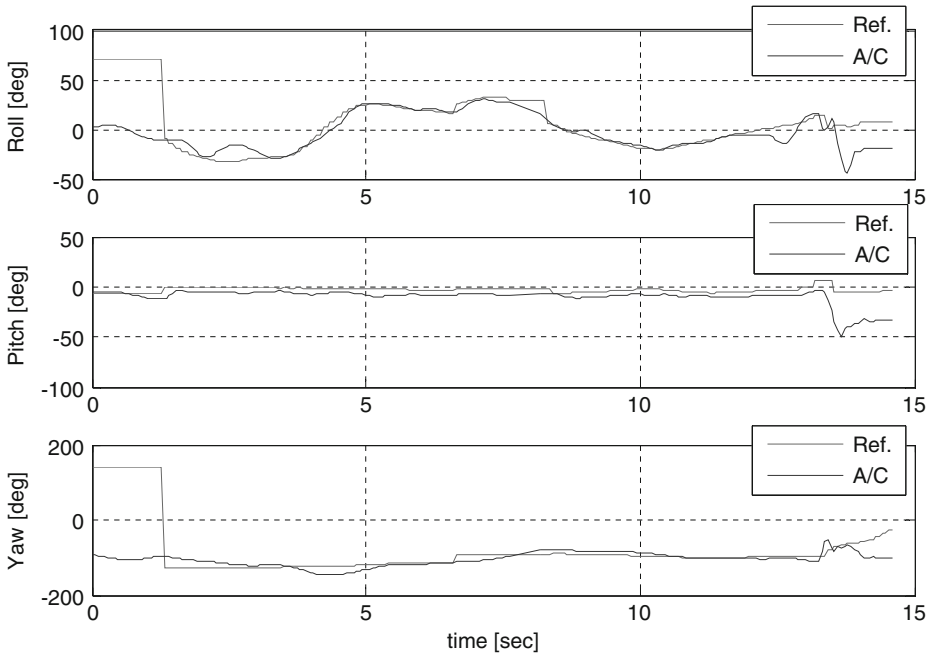

Fig. 12 Experiment result of vision-based landing: vehicle attitude and heading

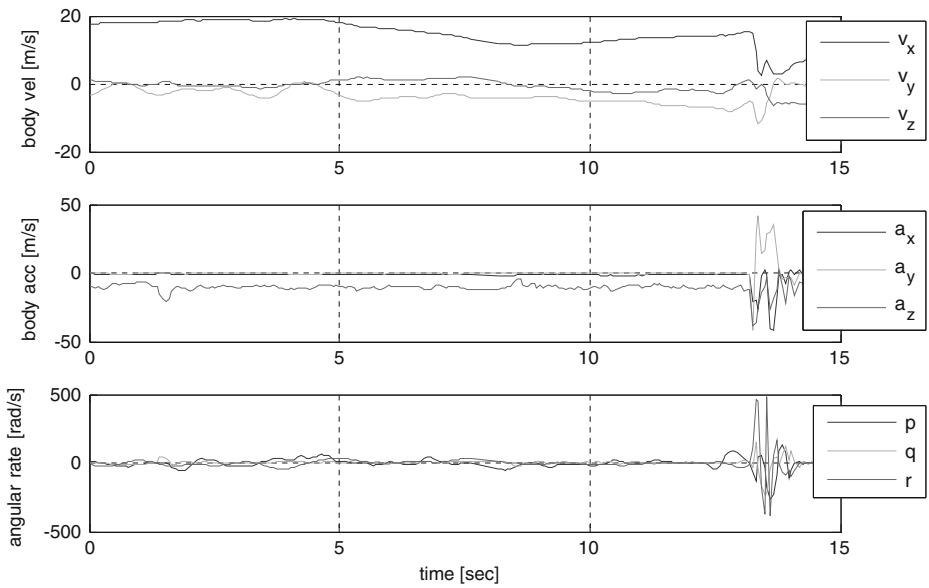

Fig. 13 Experiment result: body velocity, body acceleration and angular rate

When the heading and pitch angle errors are zero, i.e. $\Delta\psi = \Delta\theta = 0$ (the landing dome appears at the center of the image), the vehicle flies directly to the landing dome.

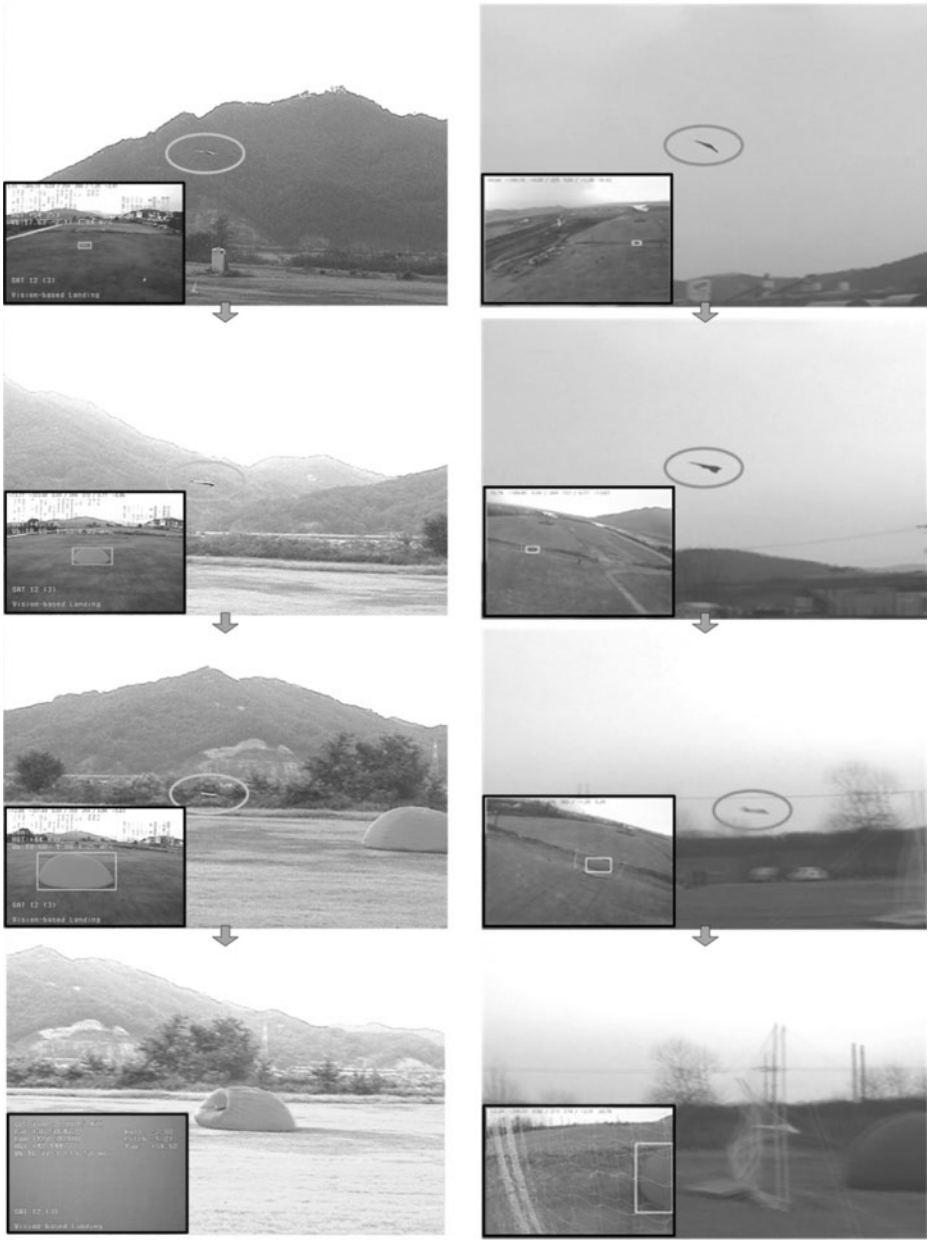

Fig. 14 Sequences of images during landing to the dome (*left*) and the recovery net (*right*)

If the camera is mounted at the nose of the airplane so that the Z^C-axis in Fig. 9 aligns with the direction of flight, any heading and pitch angle deviations indicate that the heading of the vehicle deviates from the target point. Therefore, in order to guide the vehicle to the target point, the controllers should minimize these angles. It can be done simply by sending the heading and pitch angles to the heading and pitch angle controllers. Since the pitch and yaw deviation angles computed from an image are directly sent to the controllers, the INS output is not utilized at all. This approach is simple and robust to any failure in the INS or GPS. This scheme is surprisingly simple but highly effective as will be shown in the experimental result.

4 Vision-Based Landing Experiment Result

Using the experiment setup described in Section 2, the proposed vision-based landing algorithm with landing aids was tested. First, the inflated landing dome was installed in the test field. After the GPS is locked on and the INS is initialized, the vehicle is launched using a catapult at an airspeed excess of 20 m/s. Once airborne, the vehicle is commanded to look for the landing dome in its view. When the dome is located in an image, it generates a glide slope from its current location to roughly estimated location of the dome. During descent, the aircraft flies by visual servoing, and finally, it lands at the dome or at the recovery net safely.

In Fig. 10, vehicle altitude as the results of flight test is shown. Before t = 6.6 s, the vehicle follows the glide slope leading to the roughly estimated location of the landing dome. During t = 6.6∼13.2, the vehicle flies in the direct visual servoing mode. At t = 13.2 s, the vehicle contacts with the landing net safely.

The reference altitude and the actual one are plotted in Fig. 10. The altitude of the landing dome was initially estimated to be 45 m according to reference trajectory, but it turned out to be 50 m according to the altitude of Kalman filter at the time of impact. This observation advocates our approach to use direct visual servoing instead of following blindly the initial trajectory, which does contain errors large enough to miss the landing net. Figures 11, 12, and 13 show the vehicle's 3D trajectory and states. In Fig. 14, the images taken from the onboard cameras are shown and the green rectangles in onboard images show that the landing dome was reliably detected during flight. The result also shows that the landing method using both landing dome and recovery net are feasible to recover the airplane safely.

5 Conclusion

In this paper, a vision-based automatic landing method for fixed-wing unmanned aerial vehicle is presented. The dome's distinctive color and shape provide unmistakably strong and yet passive visual cue for the onboard vision system. The vision algorithm detects the landing dome reliably from onboard images using color- and moment-based detection method. Since the onboard navigation sensors based on low-cost sensors cannot provide accurate enough navigation solutions, a direct visual servoing is implemented for precision guidance to the dome and the recovery net. The proposed idea has been validated in a series of experiments using a BWB airplane to show that the proposed system is viable approach for landing.

Acknowledgement The authors gratefully acknowledge for the financial support by Korea Ministry of Knowledge and Economy.

References

1. Williams, K.W.: A summary of unmanned aircraft accident/incident data: human factors implications. U. S. Department of Transportation Report, No. DOT/FAA/AM—04/24 (2004)
2. Manning, S.D., Rash, C.E., LeDuc, P.A., Noback R.K., McKeon, J.: The role of human causal factors in U. S. army unmanned aerial vehicle accidents. USAARL Report No. 2004—11 (2004)
3. Loegering, G.: Landing dispersion results—global Hawk auto-land system. In: AIAA's 1st Technical Conference and Workshop on Unmanned Aerial Vehicles (2002)
4. Saripalli, S., Montgomery, J.F., Sukhatme, G.S.: Vision-based autonomous landing of an unmanned aerial vehicle. In: Proceedings of the IEEE International Conference on Robotics & Automation (2002)
5. Bourquardez, O., Chaumette, F.: Visual servoing of an airplane for auto-landing. In: Proceedings of the 2007 IEEE/RSJ International Conference on Intelligent Robots and Systems (2007)
6. Trisiripisal, P., Parks, M.R., Abbott, A.L., Liu, T., Fleming, G.A.: Stereo analysis for vision-based guidance and control of aircraft landing. In: 44th AIAA Aerospace Science Meeting and Exhibit (2006)
7. Barber, B., McLain, T., Edwards, B.: Vision-based landing of fixed-wing miniature air vehicles. In: AIAA Infotech@Aerospace Conference and Exhibit (2007)
8. Hu, M.-K.: Visual pattern recognition by moment invariants. In: IRE Transactions on Information Theory (1962)
9. Flusser, J.: Moment invariants in image analysis. In: Proceedings of World Academy of Science, Engineering, and Technology (2006)